galaxies

Article

Two Dimensional Clustering of *Swift*/BAT and *Fermi*/GBM Gamma-ray Bursts

Lána Salmon [1,2,*], Lorraine Hanlon [1,2] and Antonio Martin-Carrillo [1,2]

[1] School of Physics, University College Dublin, Belfield, D04 V1W8 Dublin, Ireland; lorraine.hanlon@ucd.ie (L.H.); antonio.martin-carrillo@ucd.ie (A.M.-C.)
[2] Centre for Space Research, University College Dublin, Belfield, D04 V1W8 Dublin, Ireland
* Correspondence: lana.salmon@ucdconnect.ie

Abstract: Studies of Gamma-ray Burst (GRB) properties, such as duration and spectral hardness, have found evidence for additional classes beyond the short-hard (merger) and long-soft (collapsar) prototypes. Several clustering analyses of the duration-hardness plane identified a third, intermediate duration, class. In this work, Gaussian Mixture Model-based (GMM) clustering is applied to the *Swift*/BAT and *Fermi*/GBM samples of GRBs. The results obtained by the hierarchical combination of Gaussian components (or clusters) based on an entropy criterion are presented. This method counteracts possible overfitting arising from the application of Gaussian models to non-Gaussian underlying data. While the initial GMM clustering of the hardness-duration plane identifies three components (short/intermediate/long) for the *Swift*/BAT and *Fermi*/GBM samples, only two components (short/long) remain once the entropy criterion is applied. The analysis presented here suggests that the intermediate duration class may be the result of overfitting, rather than evidence of a distinct underlying population.

Keywords: gamma-ray burst; clustering; statistical analysis

check for updates

Citation: Salmon, L.; Hanlon, L.; Martin-Carrillo, A. Two Dimensional Clustering of *Swift*/BAT and *Fermi*/GBM Gamma-ray Bursts. *Galaxies* **2022**, *10*, 77. https://doi.org/10.3390/galaxies10040077

Academic Editors: Elena Moretti and Francesco Longo

Received: 27 April 2022
Accepted: 22 June 2022
Published: 25 June 2022

1. Introduction

The bimodal duration distribution of Gamma-ray Bursts (GRBs) suggests the separation of GRBs at $T_{90} \approx 2$ s into short/hard and long/soft classes [1]. The association of long GRBs with star forming galaxies [2] and Type Ic supernovae (Galama et al. [3], Woosley and Bloom [4]; for a review, see Cano et al. [5]) provides an observational link between long GRBs and the deaths of massive stars, supporting the collapsar scenario [6]. There is substantial evidence to support compact object mergers (neutron star–neutron star or neutron star–black hole) as the progenitors of short GRBs [7,8]. The location offsets of short GRBs from their host galaxies [9,10], their proximity to elliptical galaxies [11], and the association of GRB 170817A, an unusual short GRB, with the neutron star merger event GW 170817 detected by aLIGO [12–14], all support the merger hypothesis for the origin of short GRBs.

Other formation scenarios for short GRBs include the accretion-induced collapse of a white dwarf, double white dwarf mergers, or neutron star–white dwarf mergers [15–17], possibly leading to an unstable magnetar remnant. There are notable exceptions to the short-merger/long-collapsar paradigm, such as the short-collapsar event GRB 200826A [18–20], and GRB 060614, a long GRB without a supernova [21]. It has been suggested that many of the short duration GRBs of high redshift arise from collapsars [22]. Consideration of additional GRB characteristics, such as late X-ray flares in some short GRBs, and the non-detection of a supernova associated with some long GRBs [23], led to the suggestion of a new classification scheme [21], with Type I (massive star origin) and Type II (compact object merger origin) GRBs defined by many multiple observational criteria beyond the traditional duration and hardness [22,24]. Lü et al. [25] suggested a new parameter ϵ, based on the isotropic equivalent energy and peak energy, to classify bursts. Additionally, Donaghy et al. [26] considered 10 observational criteria for HETE-2 bursts, concluding that the best criteria to classify GRBs as 'short population' or 'long population' bursts are host galaxy properties, spectral lag, and the presence of a long-soft bump or gravitational waves.

In view of the diversity in GRB phenomenology, a definitive classification of GRBs based on duration alone is challenging. Several studies have found evidence for an additional 'intermediate' duration class of GRBs, first identified through Gaussian fits to the duration distribution of GRBs in the Third BATSE catalogue [27] and, subsequently, in fits to the GRB duration distributions of BeppoSAX [28], RHESSI [29], and *Swift* [30–35]. This class appears as an additional Gaussian 'component' required for the best-fit solution. However, the observed duration distribution can be recovered by modelling it as two skewed distributions [31,36,37], without requiring a third component.

GRB catalogues provide a set of standard parameters measured for each GRB, including duration (T_{90}), hardness ratio (HR), fluence (S), peak flux (PF), peak energy (E_{peak}), and spectral fit parameters, including the low and high energy spectral indices of the Band function [38], which fits the keV-MeV GRB spectrum, typically denoted in the literature as α and β, respectively. In the case of *Fermi*/GBM, the catalogue contains over 300 parameters for each GRB [39,40]. The availability of such large GRB catalogues allows the application of bivariate and multidimensional analyses to the data.

Table 1 summarises the previous studies, along with the resulting number of components identified for different GRB datasets. Between two and five classes of GRBs are found, depending on the sample, parameters, and methods used. Clustering of the duration-hardness plane of the final BATSE GRB catalogue identified three [41–43] or five [44–46] classes of GRBs separated by their duration, fluence, and hardness. Unsupervised neural network analysis also revealed an intermediate class [47] or two classes [48,49]. However, only two classes were found in the BATSE sample using self-organising maps [50] and fits to the duration-hardness plane with skewed bivariate distributions [51,52].

The clustering of the duration and hardness of *Swift*/BAT GRBs [53,54] and the clustering of light curve shape indicators [55] identified three classes of bursts. Gaussian Mixture Model-based (GMM) clustering applied to the *Fermi*/GBM sample revealed that GRB 170817A fit within the intermediate class in the duration-hardness plane [56], and that five classes could be identified by clustering spectral fit parameters, fluences, and durations [57]. Principal Component Analysis (PCA) also identified three classes in *Fermi*/GBM [58] and BATSE [59] samples.

Table 1. Methods and resulting components identified in clustering, fitting, and dimensionality reduction techniques applied to GRB populations. HR denotes Hardness Ratio, PF denotes Peak Flux, and S represents fluence. Studies which consider intrinsic properties such as redshift-corrected duration and hardness are marked with a *.

Study	Method	Parameters	Components
BATSE			
Horváth [27]	Fit (Gaussian)	T_{90}	3
Mukherjee et al. [41]	Clustering (Hierarchical)	T_{90}, HR, PF, S	3
Hakkila et al. [48]	Supervised pattern recognition	T_{90}, HR, PF, S, E_{peak}, α, β	2
Balastegui et al. [47]	Clustering (Hierarchical), PCA, Neural Network	T_{90}, PF, S	3
Horváth [60]	Fit (log-normal)	T_{90}	3
Rajaniemi and Mähönen [50]	Self-Organising Maps	T_{90}, HR, S	2
Hakkila et al. [49]	Clustering (k-means), Neural Network	T_{90}, HR, S	2
Chattopadhyay et al. [42]	Clustering (k-means, Dirichlet mixture)	T_{90}, HR, PF, S	3
Zitouni et al. [32]	Fit (Gaussian)	T_{90}	2
Zhang et al. [61]	Fit (Gaussian)	T_{90}	2
Bhave et al. [54]	Clustering (Gaussian Mixture-Model)	T_{90}, HR	2
Chattopadhyay and Maitra [44]	Clustering (k-means, Gaussian Mixture-Model)	T_{90}, HR, PF, S	5

Table 1. *Cont.*

Study	Method	Parameters	Components
Swift			
Kulkarni and Desai [35]	Fit (log-normal)	T_{90}	2
Chattopadhyay and Maitra [45]	Clustering (Ellipsoidal Gaussian, t-mixture)	T_{90}, PF, S	5
Tarnopolski [51]	Fit (Skewed bi-variate)	T_{90}, HR	2
Tarnopolski [52]	Fit (Skewed bi-variate)	T_{90}, HR	2
Tóth et al. [46]	Clustering (Gaussian Mixture-Model)	T_{90}, HR, PF, S	5
Modak [43]	Clustering (Fuzzy)	T_{90}, HR, PF, S	3
Horváth et al. [62]	Fit (log-normal)	T_{90}	3
Zhang and Choi [63]	Fit (log-normal)	T_{90}	2
Zhang and Choi [63] *	Fit (log-normal)	$T_{90,rest}$	2
Huja et al. [30]	Fit (Gaussian)	T_{90}	3
Huja et al. [30] *	Fit (Gaussian)	$T_{90,rest}$	1
Horváth et al. [64]	Fit (Gaussian)	T_{90}, HR	3
Veres et al. [53]	Clustering (Hierarchical, k-means)	T_{90}, HR	3
Koen and Bere [31]	Clustering (Gaussian)	T_{90}, HR	3
Tsutsui and Shigeyama [55]	Clustering (Gaussian)	Light curve shape indicators	3
Zitouni et al. [32]	Fit (Gaussian)	T_{90}	3
Zitouni et al. [32] *	Fit (Gaussian)	$T_{90,rest}$	3
Horváth and Tóth [33]	Fit (log-normal)	T_{90}	3
Tarnopolski [34]	Fit (Skew-normal)	T_{90}	3
Tarnopolski [34] *	Fit (Skew-normal)	$T_{90,rest}$	1
Yang et al. [65] *	Clustering (Gaussian Mixture-Model)	$T_{90,rest}$, HR	2
Zhang et al. [61]	Fit (Gaussian)	T_{90}	3
Zhang et al. [61] *	Fit (Gaussian)	$T_{90,rest}$	2
Bhave et al. [54]	Clustering (Gaussian Mixture-Model)	T_{90}, HR	3
Bhave et al. [54] *	Clustering (Gaussian Mixture-Model)	$T_{90,rest}$, HR	3
Kulkarni and Desai [35]	Fit (log-normal)	T_{90}	3
Kulkarni and Desai [35] *	Fit (log-normal)	$T_{90,rest}$	2
Fermi			
Zhang et al. [61]	Fit (Gaussian)	T_{90}	2
Bhave et al. [54]	Clustering (Gaussian Mixture-Model)	T_{90}, HR	2
Kulkarni and Desai [35]	Fit (log-normal)	T_{90}	2
Acuner and Ryde [57]	Clustering (Gaussian Mixture-Model)	T_{90}, S, E_{peak}, α, β	5
Horváth et al. [56]	Clustering (Gaussian Mixture-Model)	T_{90}, HR	3
Zitouni et al. [66]	Fit (Gaussian)	T_{90}	2
Zitouni et al. [66] *	Fit (Gaussian)	$T_{90,rest}$	2
Horváth et al. [58]	Principal Component Analysis	T_{90}, PF, S, E_{peak}, α, β	3
Tarnopolski [51]	Fit (skewed bivariate)	T_{90}, HR	2
BeppoSAX			
Horváth [28]	Fit (log-normal)	T_{90}	3
Kulkarni and Desai [35]	Fit (log-normal)	T_{90}	2
RHESSI			
Řípa et al. [29]	Fit (log-normal)	T_{90}	2
Řípa et al. [29]	Fit (log-normal)	T_{90}, HR	3
Řípa et al. [67]	Clustering (Gaussian Mixture-Model, k-means)	T_{90}, HR	3
INTEGRAL			
Minaev et al. [68]	Fit (log-normal)	T_{90}	2
Konus-Wind			
Svinkin et al. [69]	Fit (log-normal)	T_{50}	2
Svinkin et al. [69]	Clustering (Gaussian Mixture Model)	T_{50}, HR	3
Multiple samples			
Minaev and Pozanenko [70] *	Fit (Skew-normal)	$T_{90,rest}$, E_{iso}, $E_{peak,rest}$	2

Observational bias has been suggested as a possible origin of the putative intermediate class. Bias caused by short temporal trigger windows favours short low-fluence bursts (fluence-duration bias; Hakkila et al. [49]), while the low signal-to-noise ratios of long faint bursts can cause them to be mistaken for short bursts ('tip-of-the-iceberg' effect; Lü et al. [71]). However, neither of these effects have been able to reproduce the third class in simulations. It has been shown that the third class can arise as a consequence of fitting symmetrical models to the GRB duration distribution, which may be skewed rather than symmetrical [31,36,37,51], possibly as a result of the GRB pulse shapes [72].

The significant number of GRBs with measured redshift in the *Swift* and *Fermi* samples has allowed studies of intrinsic properties, which have pointed to the existence of two classes in the *Fermi*/GBM sample [32]. For the *Swift*/BAT sample of bursts, one [30,34], two [35,61,63,65], or three [32,54] classes have been identified. However, cosmological time dilation applied to GRB durations has not been found to transform a rest-frame two-component Gaussian duration distribution to the observed skewed one [73]. While there are now more than 400 *Swift* GRBs with measured redshift, there are only 25 short duration bursts with $T_{90,\mathrm{obs}} < 2\,\mathrm{s}$. The rest-frame studies outlined in Table 1 note that the short duration sample is not statistically significant, and a larger sample is required [54,65].

This paper reports on an updated two-dimensional clustering analysis in the duration-hardness plane of the large *Fermi*/GBM and *Swift*/BAT GRB samples. Advancing previous studies, the analysis presented here makes use of an entropy criterion to identify 'excess' components that may be identified in the standard GMM clustering of data but which arise from the application of Gaussian models to non-Gaussian underlying data [74]. This method has been applied in other astrophysical contexts, for example in the clustering of stars [75]. As the number of short GRBs with redshift has not grown significantly since previous studies, this paper focuses on GMM clustering using observed, rather than intrinsic, properties.

Section 2 outlines the sample construction, while Section 3 provides details of the methods applied to perform clustering. The results and discussion are presented in Sections 4 and 5 respectively, while the conclusions are outlined in Section 6.

2. Datasets and Data Preparation

2.1. *Swift/BAT*

The Third *Swift*/BAT Catalogue [76] contains 1388 bursts detected between 17 December 2004 and 28 August 2020 and provides the durations, spectral fit parameters, fluxes, and fluences calculated in the simple Power-Law (PL) and Cut-off Power-Law (CPL) models. The hardness ratio HR_{32} for each GRB was calculated as the ratio of the fluence in energy range 3 (50–100 keV) to energy range 2 (25–50 keV), given by

$$\mathrm{HR}_{32} = \frac{\int_{50\,\mathrm{keV}}^{100\,\mathrm{keV}} E f(E) dE}{\int_{25\,\mathrm{keV}}^{50\,\mathrm{keV}} E f(E) dE}, \tag{1}$$

where $f(E)$ is the photon flux at energy E. For the PL model, this is given by

$$f(E) = K_{50}^{\mathrm{PL}} \left(\frac{E}{50\ \mathrm{keV}} \right)^{\alpha^{\mathrm{PL}}}, \tag{2}$$

where α^{PL} is the PL index, and K_{50}^{PL} is the normalisation factor at 50 keV, with units of photons cm^{-2} s^{-1} keV^{-1}. The CPL model is described as

$$f(E) = K_{50}^{\mathrm{CPL}} \left(\frac{E}{50\ \mathrm{keV}} \right)^{\alpha^{\mathrm{CPL}}} \exp\left(\frac{-E(2+\alpha^{\mathrm{CPL}})}{E_{\mathrm{peak}}} \right), \tag{3}$$

where α^{CPL} is the CPL index, K_{50}^{CPL} is the normalisation factor at 50 keV, with units of photons cm^{-2} s^{-1} keV^{-1}, and E_{peak} is the peak energy in keV of the νF_ν or $E^2 f(E)$ spectrum.

This is the flux density integrated over the energy range, also known as the spectral flux density.

The sample of 1388 bursts was filtered to remove 52 GRBs for which no duration or best-fit model was documented. A further 20 GRBs with duration or hardness errors in excess of 50% of their magnitude were removed, resulting in a final sample of 1316 GRBs for clustering.

2.2. Fermi/GBM

The *Fermi*/GBM catalogue was accessed using the *Fermi*/GBM Data Tools [40] and limited to the period between 10 August 2008 and 17 March 2021, which yielded a sample of 3001 bursts. The hardness ratio was calculated by comparing the counts detected in the 8–50 keV band to the 50–300 keV band. Counts within the T_{90} interval were summed from the 64 ms light curves, generated using Time-Tagged Event (TTE) data in the *Fermi*/GBM Data Tools. Only triggered detectors were used, and the background subtraction was performed using the background intervals defined in the *Fermi*/GBM catalogue. Bursts with no documented duration or incorrect background subtraction were removed, resulting in a sample of 2669 bursts. Prior to clustering, 36 outliers were identified by the R package `HDOutliers` [77] and removed from the sample, leaving a final sample of 2633 bursts for clustering.

3. Clustering Methods

3.1. GMM Clustering

GMM clustering was carried out in R using the MCLUST [78]. GMM clustering assumes that the observed data are generated from a mixture of K components, where the density of each component is described by a multivariate Gaussian distribution. MCLUST fit 14 different models to the data, parameterised by the shape (spherical or ellipsoidal) and volume. In the case of ellipsoidal models, the alignment of the axes and the difference in shape of the fitted ellipsoidals was specified. This is known as Volume-Shape-Orientation (VSO) decomposition. For a given model, the volume, shape, and orientation can be constrained to equal variance, denoted by 'E'. If the variance is free to change, the model is denoted 'V'. Additionally, the orientation of the clusters relative to each other can be constrained to Equal or Varying, or a model can have alignment limited to the coordinate axis, and is labelled 'I'. For example, 'EVI' denotes equal volume components, with variable shapes (i.e., not spherical) and orientation aligned with the axes.

MCLUST makes use of the Bayesian Information Criterion (BIC; Schwarz et al. [79]) to compare mixture models fitted on the data. The best-fit model and number of components are chosen based on the largest BIC value. A difference in BIC value between models of 6–10 is considered significant, while a difference of greater than 2 provides positive evidence for a better fit [80]. This standard GMM fit method is the same as that employed in some previous studies, for example Horváth et al. [56] and Bhave et al. [54].

3.2. Combination of Gaussian Components

In the case where Gaussian components were overlapping or components were suspected to be non-Gaussian, as has been shown for the BATSE and *Fermi*/GBM GRB duration distributions [51,52], the MCLUST function `clustCombi` was used to hierarchically combine components using an entropy criterion [74]. Entropy is a measure of the uncertainty of the observations belonging to a certain cluster or component. Thus, a large decrease in entropy signifies a better fit with smaller uncertainty. For MCLUST, the final number of components was chosen based on the observed 'elbow' in the entropy plot. The number of components at which the elbow occurred pointed to a large decrease in entropy and, therefore, a model with smaller uncertainty.

There are several methods for joining Gaussian Mixture components. In comparison to the entropy criterion, these methods have limitations, for example, requiring spherical components [81] or one-dimensional data [82]. Other suggested methods assume the number of clusters [83] or make use of hard clustering methods, which assigns points to one cluster rather than applying a probabilistic method (e.g., Tantrum et al. [84]). The method employed in this study was a soft-clustering probabilistic method, which is computationally efficient and applicable to multiple dimensions. Hence, it was the chosen method to achieve a robust clustering result for the complex GRB datasets.

4. Results

The results of the initial MCLUST fit and subsequent `clustCombi` method applied to the *Swift*/BAT and *Fermi*/GBM samples are summarised in Table 2.

Table 2. Number of components (K), Bayesian Information Criterion (BIC) values, models, and number of bursts (#) identified in the MCLUST and subsequent `clustCombi` fits to the *Swift*/BAT and *Fermi*/GBM samples.

	Initial MCLUST Fit			`clustCombi` Fit		
	Model	**K**	**BIC**	**K**	**# Short**	**# Long**
Swift/BAT	VEI	3	−720	2	85	1231
Fermi/GBM	VEI	3	−3970	2	295	2338

4.1. *Swift/BAT*

The BIC values for the top three models versus the number of components, resulting from the application of MCLUST to the full *Swift*/BAT sample, are shown in Figure 1a. The 'VEI' model with three components had the largest BIC value. The three components were labelled 'long', 'intermediate', and 'short' according to their durations and are projected onto the hardness-duration plane in Figure 1b. The clear round edge between the intermediate and long components suggests that a Gaussian was being fit to a non-Gaussian component.

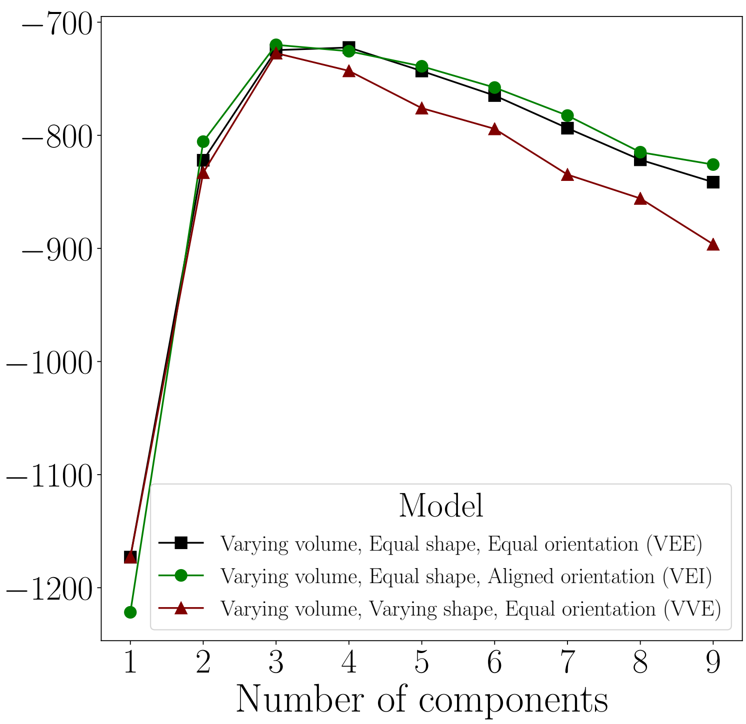

(**a**)

Figure 1. *Cont.*

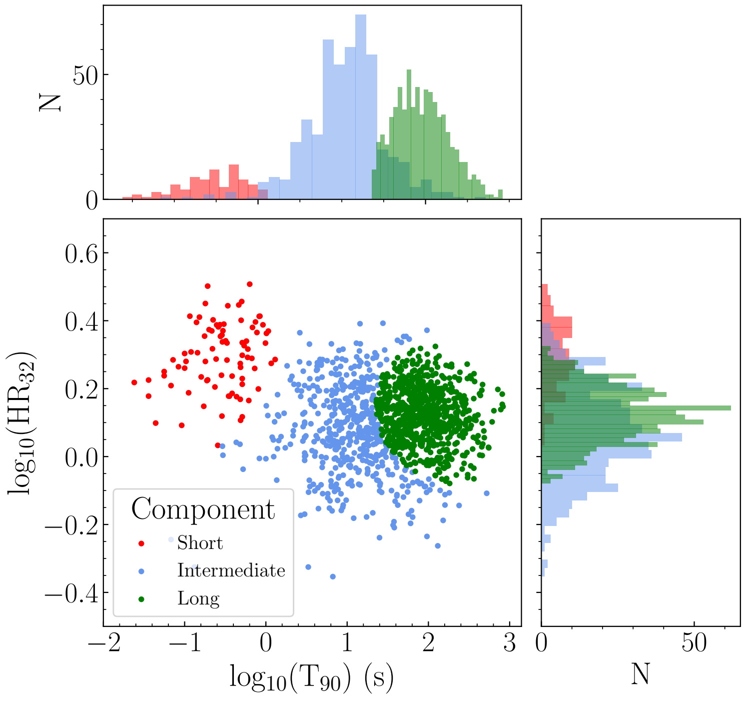

(**b**)

Figure 1. (**a**) BIC values of the top three MCLUST models fit to the *Swift*/BAT sample and (**b**) the resulting duration-hardness plane for the best-fit three-component model (VEI).

After `clustCombi` was applied, the 'intermediate' and 'long' components were combined, producing a large decrease in entropy as shown in Figure 2. The two remaining components or classes were labelled 'long' and 'short', as shown in Figure 3. Table 2 presents the sample size of the classes.

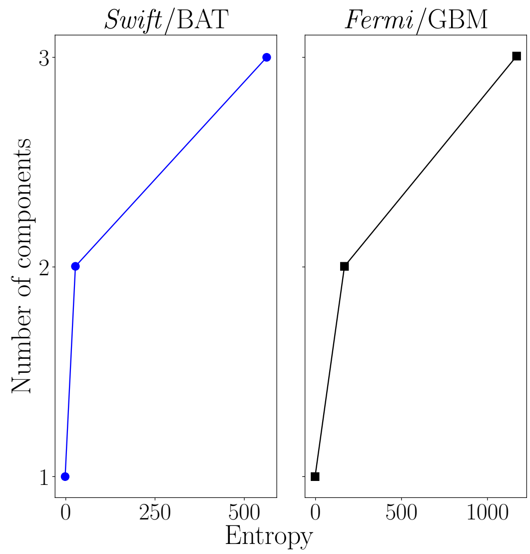

Figure 2. Entropy plots returned by `clustCombi` depicting the entropy of the initial MCLUST fits (three components) and the entropy after combination of the initial MCLUST components for *Swift*/BAT (left) and *Fermi*/GBM (right). An inflection, or elbow, in the entropy plot signifies a model with the optimal number of components.

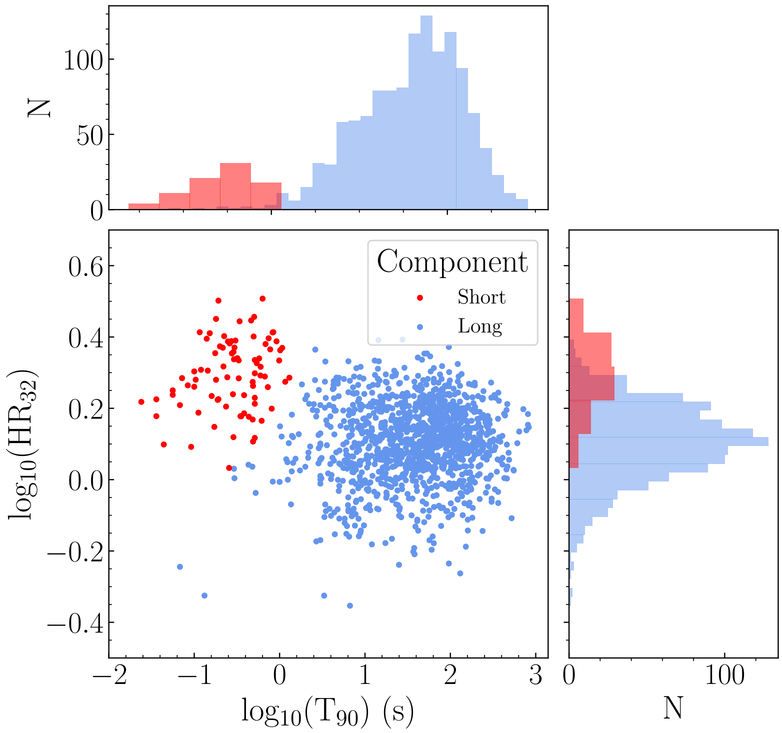

Figure 3. The results of `clustCombi` applied to the components identified by MCLUST in the duration-hardness plane for *Swift*/BAT.

The distributions of the duration (T_{90}) and hardness ratio (HR_{32}) are depicted in the violin plot in Figure 4. The mean, standard deviation, and median values of these parameters for the long and the short classes are presented in Table 3.

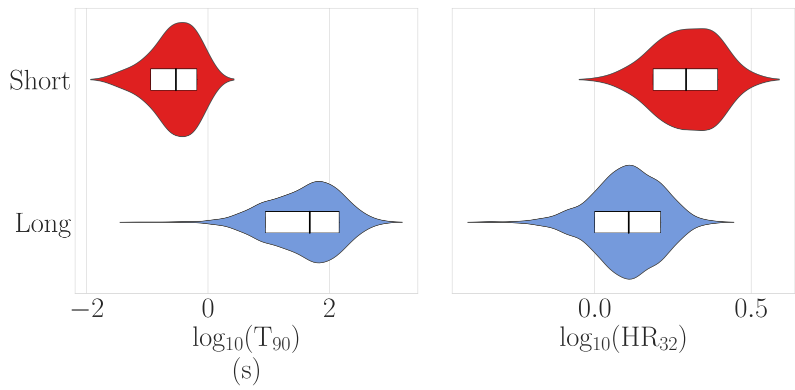

Figure 4. Violin plots showing the distribution of the duration (T_{90}) and hardness ratio (HR_{32}) for the *Swift*/BAT 'short' (red) and 'long' (blue) classes identified by `clustCombi`. The median of each parameter is marked as a black line within the box, which represents the 1 σ interval (i.e., the 16th to 84th percentile).

Table 3. Mean (μ), standard deviation (σ), and median of the properties of the *Swift*/BAT 'long' and 'short' classes identified by `clustCombi`.

	Short			**Long**		
	μ	σ	**Median**	μ	σ	**Median**
T_{90} (s)	0.39	0.29	0.30	79.8	101.0	47.7
HR_{32}	2.02	0.46	1.96	1.31	0.32	1.28

4.2. *Fermi*/GBM

For *Fermi*/GBM, the initial MCLUST fit indicated that a three-component fit to the data was preferred. The BIC values of the top three models are shown in Figure 5a. The three best-fit components are depicted in Figure 5b. The three-component 'VEI' model exhibited a BIC value difference of ∼6 compared to the next best model; thus, it was considered a significant result. The classification components were labelled 'short', 'intermediate', and 'long', according to their duration. The boundary between the 'intermediate' and 'long' components exhibited a similar round-edge feature as identified in the results for *Swift*/BAT.

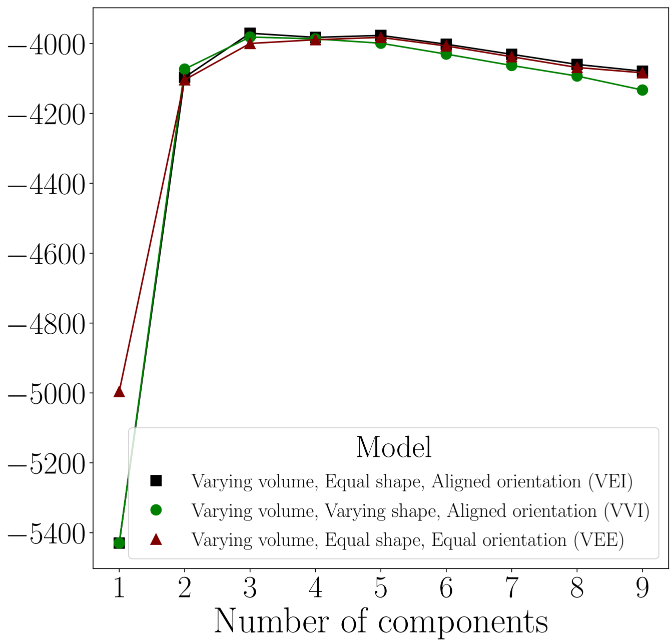

(**a**)

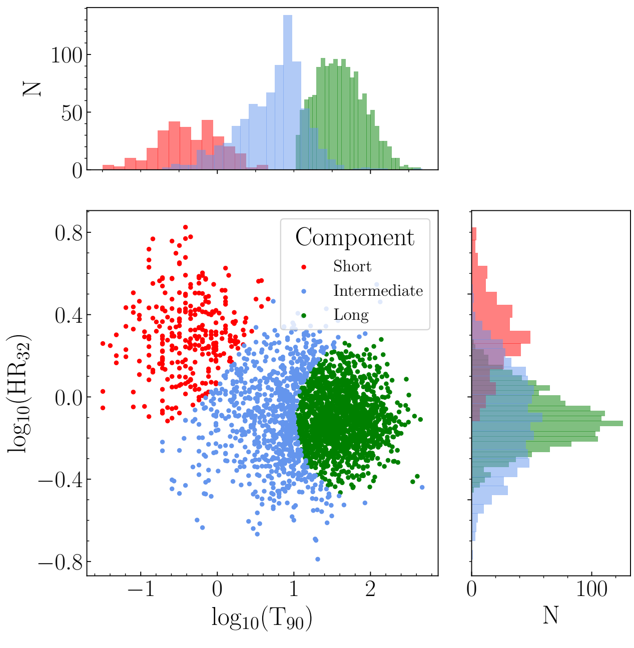

(**b**)

Figure 5. (**a**) BIC values of the top three MCLUST models fit to the *Fermi*/GBM sample and (**b**) the resulting duration-hardness plane for the best-fit three-component model (VEI).

The results obtained from applying `clustCombi` to this sample are shown in Figure 6, indicating that a model consisting of two components or classes, rather than three, provided a better fit to the data, based on a decrease in entropy depicted in the entropy plot in Figure 2. The number of bursts in the 'long' and 'short' classes identified by `clustCombi` is presented in Table 2.

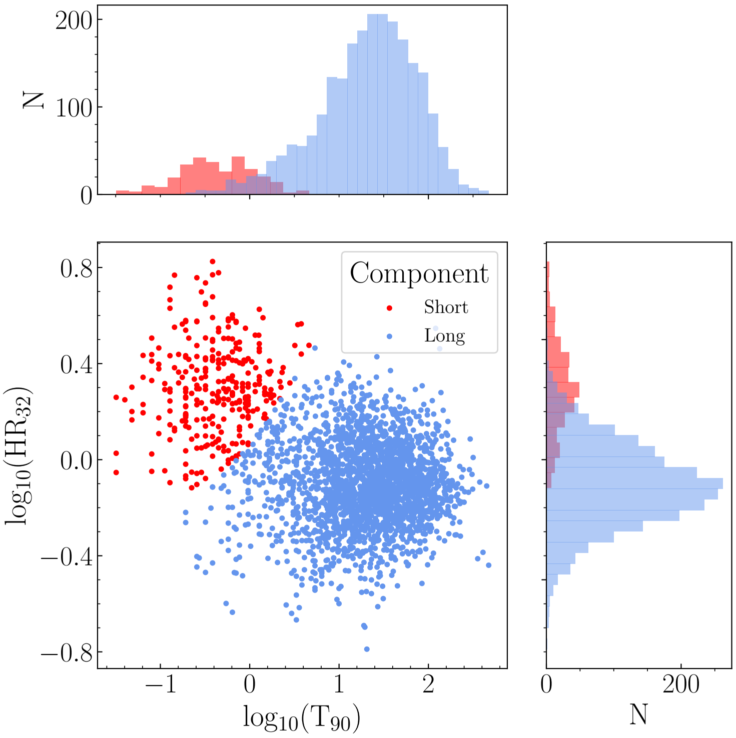

Figure 6. The results of `clustCombi` applied to the components identified by MCLUST in the duration-hardness plane for *Fermi*/GBM.

The violin plot in Figure 7 for the *Fermi*/GBM sample demonstrates the distributions of the duration and hardness ratio, while the summary statistics of these populations are presented in Table 4.

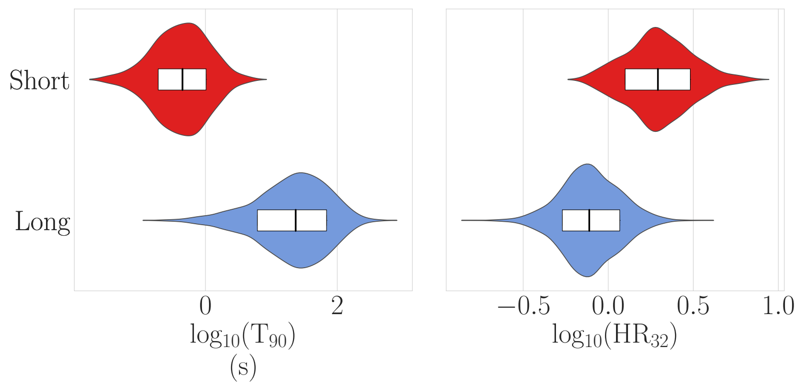

Figure 7. Violin plots showing the distribution of the duration (T_{90}) and hardness ratio (HR_{32}) for the *Fermi*/GBM 'short' (red) and 'long' (blue) classes identified by `clustCombi`. The median of each parameter is marked as a black line within the box, which represents the 1 σ interval (i.e., the 16th to 84th percentile).

Table 4. Mean (μ), standard deviation (σ), and median of the properties of the *Fermi*/GBM 'long' and 'short' classes identified by `clustCombi`.

	Short			Long		
	μ	σ	**Median**	μ	σ	**Median**
T_{90} (s)	0.64	0.65	0.45	38.6	23.4	45.4
HR_{32}	1.99	1.53	1.96	0.78	1.49	0.77

5. Discussion

5.1. *Swift/BAT*

For *Swift*/BAT, the three components identified in Figure 1b had a similar size and structure to those identified in the GMM clustering by Bhave et al. [54]. In this analysis, the hardness ratio was computed using the best-fit model for *Swift*, consistent with the method undertaken by Bhave et al. [54], enabling comparison of results. The clear-cut round boundary between the intermediate and long components in Figure 1b was also found by Bhave et al. [54] and is a signature of the application of a Gaussian model to a non-Gaussian underlying distribution.

The result of applying `clustCombi` after the GMM clustering indicated that the intermediate duration component, combined with the long duration component, provided a better fit to the sample of *Swift*/BAT bursts (Figure 3). Thus, the intermediate class was likely identified by the overfitting resulting from GMM clustering applied to the complex distribution of *Swift*/BAT bursts in duration-hardness space.

Figure 4 and Table 3 show that the mean duration of the short class identified by `clustCombi` was $T_{90} \approx 0.3$ s (1 σ standard deviation of 0.29 s), while the long class had a mean $T_{90} \approx 70$ s (1 σ standard deviation of 101 s). This is consistent with the peaks of the *Swift* short ($T_{90} < 2$ s) and long ($T_{90} > 2$ s) duration distributions [85]. The shorter duration class had a larger hardness ratio than the longer duration class, as expected from the traditional short/long paradigm. The separation between the short and long classes occurred at $T_{90} \approx 0.5$–2 s. This is in agreement with the findings of Bromberg et al. [86], whose modelling of the duration distribution of *Swift*/BAT bursts using the Collapsar model suggested a separation at $T_{90} \approx 0.8$ s.

5.2. *Fermi/GBM*

Prior to the removal of the 36 outlier bursts, MCLUST initially suggested a fit with four components in the *Fermi*/GBM sample. The fit included one group of bursts with very high or very low hardness ratios situated in a halo around the three groups in Figure 5b. These outlier bursts were effectively removed using `HDOutliers` (Section 2), following previous studies including Tóth et al. [46], Horváth et al. [56,58] and were likely the result of unsuitable background subtraction. Upon removal of the outliers, MCLUST identified three components, which were similar to the components obtained for *Swift*/BAT (Figure 5b). The intermediate duration component contained more bursts than the class identified by Horváth et al. [56], whose intermediate class only contained bursts with low spectral hardness. This difference can be attributed to their smaller sample size of 1298 bursts.

A signature of a Gaussian component is visible at the sharp boundary between the intermediate and long duration components in Figure 5b, indicating an arbitrary Gaussian component was identified. Consistent with the results obtained for *Swift*/BAT, the intermediate component was disregarded when `clustCombi` was applied, indicating that it was likely an overfitting component identified by the GMM clustering procedure. Thus, a short and long duration class remained.

In this analysis, the hardness ratio was computed using the background-subtracted counts to be consistent with previous *Fermi*/GBM studies and to enable direct comparison with those results. The short and long duration classes in Figure 6 were comparable to the classes found in previous GMM clustering analyses by Bhave et al. [54], Bhat et al. [87], and in skewed bi-variate fits carried out by Tarnopolski [51]. Table 4 and Figure 7 show that the short duration class was spectrally harder than the long duration class, as expected. The mean duration of the classes were 0.64 s (1 σ standard deviation of 0.65 s) and 38.6 s (1 σ standard deviation of 23.4 s) for the short and long classes, respectively. This result is consistent with the mean durations of the short (0.82 s) and long (28.3 s) classes identified in the GMM clustering of the third *Fermi*/GBM catalogue [87].

5.3. Comparison to GRB Subclasses

Groups 1 and 2 of the *Swift*/BAT and *Fermi*/GBM samples resemble the traditional short/hard and long/soft prototypes. The groups can be compared to several subclasses of GRBs, including those with associated supernovae, extended emission episodes, and plateaus. The longer duration Group 2 contained all 49 bursts with an X-ray plateau from the platinum sample identified by Dainotti et al. [88]. Similarly, all bursts in the sample with an optical plateau [89] and those with an associated supernova and a plateau [90] lay in Group 2. The *Swift* sample analysed also contained four ultra-long GRBs from the Gold sample and five possible ultra-long GRBs from the Silver sample of Gendre et al. [91]. All of these bursts resided in Group 2 as expected, given their duration.

Short GRBs with extended emission episodes have challenged the typical duration-based classification scheme of GRBs. The population of *Swift* GRBs with extended emission identified by Gibson et al. [92] contains bursts chosen from the sample in Kaneko et al. [93] and Gompertz et al. [94,95]. The Gibson et al. [92] sample was found to only contain bursts from Group 2 of our *Swift*/BAT results. This is understandable, given that the rebrightening exhibited in their light curves can lead to an increase in the measured T_{90} [70], thus placing them in Group 2. The extended emission episodes are typically softer than the initial spike, dominating the overall detected fluence, thus resulting in a longer duration GRB.

Group 2 resembled the standard long-duration group for both the *Swift* and *Fermi* samples. Thus, bursts with associated supernovae were expected to belong to this group. The sample of supernova-associated GRBs from Cano et al. [5] was updated to include more recent events GRB 161219B/SN 2016jca [96], GRB 171205A/SN 2017htp [97], GRB 180728A/SN 2018fip [98,99], GRB 190114C/SN 2019jrj and GRB 190829A/AT2019oyw [100], and GRB 200826A [18–20]. There were 25 *Swift* and 15 *Fermi* GRB-SN cases within the sample analysed, all of which resided in Group 2 as expected. The only confirmed GRB with a kilonova, GRB 170817, was also in Group 1 of the *Fermi* sample.

5.4. Selection Effects

Svinkin et al. [69] suggested that T_{50}, the time during which 50% of the counts above background are recorded, is a more robust duration measure than T_{90}, since it may be less affected by detector energy ranges. To eliminate possible selection effects and to verify the two-component solutions, the clustering analysis was repeated using T_{50} as the duration parameter. For *Swift*/BAT, the initial MCLUST fit returned a three-component solution similar to Figure 1b—the short duration group remained the same, while the two long duration groups also exhibited the clear-cut spherical feature identified in the T_{90} analysis. When `clustCombi` was applied, a two group-solution was the best fit. Group 1 and Group 2 were identical to the groups found in the T_{90} analysis. Thus, for *Swift*/BAT, this method did not favour T_{50} over T_{90} as a duration measure, and the results further supported the two-group solution.

For *Fermi*/GBM, the initial MCLUST fit identified an extra long duration group in a four-component solution. The long duration group in Figure 5b was split in two, with the remaining structure matching the results of the T_{90} analysis. `clustCombi` resulted in a two-component fit closely resembling the structure and makeup of Group 1 and Group 2 of the T_{90} fit. However, Group 1 contained ≈ 100 more GRBs than the T_{90} fit. For *Fermi*/GBM, the two-component fit was supported, and while the T_{50} parameter returned slightly different proportions in each group, it did not demonstrate any clear advantage over T_{90} as a duration parameter.

6. Conclusions

GMM clustering with MCLUST identified three Gaussian components of *Swift*/BAT and *Fermi*/GBM bursts in the duration-hardness plane. The third component resembled the intermediate duration group identified in previous studies. However, combining components, based on an entropy criterion, identified a short and long duration class only for both samples.

This study highlights the drawbacks of fitting GRB populations with model-based methods. Similar model-based fitting methods, including the log-normal fit procedures applied to GRB duration distributions, have exhibited components thought to be identified incorrectly due to the inherently skewed distribution of long GRB durations [31,36]. Table 1 highlights the diversity of results from model-based studies.

The lack of consensus regarding a definitive number of GRB classes, both in the analysis presented here and in previous studies of GRB catalogues, is a motivator for a model-independent analysis of GRB light curves. The light curves may also contain more information than the summary data provided by the GRB catalogues. Fourier analysis of the *Swift*/BAT GRB light curves by Jespersen et al. [101] identified two classes of bursts. Following on from the analysis presented in this paper is a wavelet-based feature extraction analysis of GRB light curves from *Swift*/BAT, BATSE and *Fermi*/GBM (Salmon et al. [102], in preparation).

Author Contributions: Conceptualization, L.S., L.H. and A.M.-C.; methodology, L.S., L.H. and A.M.-C.; software, L.S.; validation, L.S., L.H. and A.M.-C.; formal analysis, L.S.; investigation, L.S.; resources, L.S., L.H. and A.M.-C.; data curation, L.S.; writing—original draft preparation, L.S.; writing—review and editing, L.H. and A.M.-C.; visualization, L.S.; supervision, L.H. and A.M.-C. ; project administration, L.H. and A.M.-C.; funding acquisition, L.H. and A.M.-C. All authors have read and agreed to the published version of the manuscript.

Funding: L.S. acknowledges the Irish Research Council Postgraduate Scholarship No GOIPG/2017/1525. L.H. acknowledges support from Science Foundation Ireland (Grant number 19/FFP/6777) and the EU H2020 (Grant agreement 871158).

Institutional Review Board Statement: Not applicable.

Informed Consent Statement: Not applicable.

Data Availability Statement: This paper makes use of the *Swift*/BAT catalogue [76], which can be accessed through the online *Swift*/BAT Gamma-ray Burst Catalogue [1]. The *Fermi*/GBM catalogue is accessed through the *Fermi*/GBM data tools [40].

Acknowledgments: This research made use of the following Python packages: NumPy [103], Matplotlib [104] and pandas [105,106]. The authors are grateful to Brendan Murphy and Michael Fop for their assistance with MCLUST.

Conflicts of Interest: The authors declare no conflict of interest. The funders had no role in the design of the study; in the collection, analyses, or interpretation of data; in the writing of the manuscript, or in the decision to publish the results.

Note

[1] https://swift.gsfc.nasa.gov/results/batgrbcat/, (accessed on 16 June 2022).

References

1. Kouveliotou, C.; Meegan, C.A.; Fishman, G.J.; Bhat, N.P.; Briggs, M.S.; Koshut, T.M.; Paciesas, W.S.; Pendleton, G.N. Identification of Two Classes of Gamma-ray Bursts. *Astrophys. J.* **1993**, *413*, L101. [CrossRef]
2. Perley, D.A.; Niino, Y.; Tanvir, N.R.; Vergani, S.D.; Fynbo, J.P.U. Long-Duration Gamma-ray Burst Host Galaxies in Emission and Absorption. *Space Sci. Rev.* **2016**, *202*, 111–142. [CrossRef]
3. Galama, T.J.; Vreeswijk, P.M.; van Paradijs, J.; Kouveliotou, C.; Augusteijn, T.; Böhnhardt, H.; Brewer, J.P.; Doublier, V.; Gonzalez, J.F.; Leibundgut, B.; et al. An unusual supernova in the error box of the γ-ray burst of 25 April 1998. *Nature* **1998**, *395*, 670–672. [CrossRef]

4. Woosley, S.E.; Bloom, J.S. The Supernova Gamma-ray Burst Connection. *Annu. Rev. Astron. Astrophys.* **2006**, *44*, 507–556. [CrossRef]
5. Cano, Z.; Wang, S.Q.; Dai, Z.G.; Wu, X.F. The Observer's Guide to the Gamma-ray Burst Supernova Connection. *Adv. Astron.* **2017**, *2017*, 8929054, [CrossRef]
6. MacFadyen, A.I.; Woosley, S.E. Collapsars: Gamma-ray Bursts and Explosions in "Failed Supernovae". *Astrophys. J.* **1999**, *524*, 262–289. [CrossRef]
7. Eichler, D.; Livio, M.; Piran, T.; Schramm, D.N. Nucleosynthesis, neutrino bursts and γ-rays from coalescing neutron stars. *Nature* **1989**, *340*, 126–128. [CrossRef]
8. Narayan, R.; Paczynski, B.; Piran, T. Gamma-ray Bursts as the Death Throes of Massive Binary Stars. *Astrophys. J.* **1992**, *395*, L83. [CrossRef]
9. Berger, E. A Short Gamma-ray Burst "No-host" Problem? Investigating Large Progenitor Offsets for Short GRBs with Optical Afterglows. *Astrophys. J.* **2010**, *722*, 1946–1961. [CrossRef]
10. Tunnicliffe, R.L.; Levan, A.J.; Tanvir, N.R.; Rowlinson, A.; Perley, D.A.; Bloom, J.S.; Cenko, S.B.; O'Brien, P.T.; Cobb, B.E.; Wiersema, K.; et al. On the nature of the 'hostless' short GRBs. *Mon. Not. R. Astron. Soc.* **2014**, *437*, 1495–1510. [CrossRef]
11. Berger, E. Short-Duration Gamma-ray Bursts. *Annu. Rev. Astron. Astrophys.* **2014**, *52*, 43–105. [CrossRef]
12. Abbott, B.P.; Abbott, R.; Abbott, T.D.; Acernese, F.; Ackley, K.; Adams, C.; Adams, T.; Addesso, P.; Adhikari, R.X.; Adya, V.B.; et al. Multi-messenger Observations of a Binary Neutron Star Merger. *Astrophys. J.* **2017**, *848*, L12. [CrossRef]
13. Goldstein, A.; Veres, P.; Burns, E.; Briggs, M.S.; Hamburg, R.; Kocevski, D.; Wilson-Hodge, C.A.; Preece, R.D.; Poolakkil, S.; Roberts, O.J.; et al. An Ordinary Short Gamma-ray Burst with Extraordinary Implications: Fermi-GBM Detection of GRB 170817A. *Astrophys. J.* **2017**, *848*, L14. [CrossRef]
14. Savchenko, V.; Ferrigno, C.; Kuulkers, E.; Bazzano, A.; Bozzo, E.; Brandt, S.; Chenevez, J.; Courvoisier, T.L.; Diehl, R.; Domingo, A.; et al. INTEGRAL detection of the first prompt gamma-ray signal coincident with the gravitational-wave event GW170817. *Astrophys. J.* **2017**, *848*, L15. [CrossRef]
15. Qin, B.; Wu, X.P.; Chu, M.C.; Fang, L.Z.; Hu, J.Y. The Collapse of Neutron Stars in High-Mass Binaries as the Energy Source for the Gamma-ray Bursts. *Astrophys. J.* **1998**, *494*, L57–L59. [CrossRef]
16. Levan, A.J.; Wynn, G.A.; Chapman, R.; Davies, M.B.; King, A.R.; Priddey, R.S.; Tanvir, N.R. Short gamma-ray bursts in old populations: Magnetars from white dwarf-white dwarf mergers. *Mon. Not. R. Astron. Soc. Lett.* **2006**, *368*, L1–L5. [CrossRef]
17. Metzger, B.D.; Quataert, E.; Thompson, T.A. Short-duration gamma-ray bursts with extended emission from protomagnetar spin-down. *Mon. Not. R. Astron. Soc. Lett.* **2008**, *385*, 1455–1460. [CrossRef]
18. Ahumada, T.; Singer, L.P.; Anand, S.; Coughlin, M.W.; Kasliwal, M.M.; Ryan, G.; Andreoni, I.; Cenko, S.B.; Fremling, C.; Kumar, H.; et al. Discovery and confirmation of the shortest gamma ray burst from a collapsar. *arXiv* **2021**, arXiv:2105.05067.
19. Rossi, A.; Rothberg, B.; Palazzi, E.; Kann, D.A.; D'Avanzo, P.; Klose, S.; Perego, A.; Pian, E.; Savaglio, S.; Stratta, G.; et al. The peculiar short-duration GRB 200826A and its supernova. *arXiv* **2021**, arXiv:2105.03829.
20. Zhang, B.B.; Liu, Z.K.; Peng, Z.K.; Li, Y.; Lü, H.J.; Yang, J.; Yang, Y.S.; Yang, Y.H.; Meng, Y.Z.; Zou, J.H.; et al. A Peculiarly Short-duration Gamma-ray Burst from Massive Star Core Collapse. *arXiv* **2021**, arXiv:2105.05021.
21. Zhang, B.; Zhang, B.B.; Liang, E.W.; Gehrels, N.; Burrows, D.N.; Mészáros, P. Making a Short Gamma-ray Burst from a Long One: Implications for the Nature of GRB 060614. *Astrophys. J.* **2007**, *655*, L25–L28. [CrossRef]
22. Zhang, B.; Zhang, B.B.; Virgili, F.J.; Liang, E.W.; Kann, D.A.; Wu, X.F.; Proga, D.; Lv, H.J.; Toma, K.; Mészáros, P.; et al. Discerning the Physical Origins of Cosmological Gamma-ray Bursts Based on Multiple Observational Criteria: The Cases of z = 6.7 GRB 080913, z = 8.2 GRB 090423, and Some Short/Hard GRBs. *Astrophys. J.* **2009**, *703*, 1696–1724. [CrossRef]
23. Hjorth, J.; Bloom, J.S. The Gamma-ray Burst—Supernova Connection. In *Gamma-ray Bursts*; Cambridge University Press: Cambridge, MA, USA, 2012; Chapter 9, pp. 169–190.
24. Li, Y.; Zhang, B.; Yuan, Q. A Comparative Study of Long and Short GRBs. II. A Multiwavelength Method to Distinguish Type II (Massive Star) and Type I (Compact Star) GRBs. *Astrophys. J.* **2020**, *897*, 154. [CrossRef]
25. Lü, H.J.; Liang, E.W.; Zhang, B.B.; Zhang, B. A New Classification Method for Gamma-ray Bursts. *Astrophys. J.* **2010**, *725*, 1965–1970. [CrossRef]
26. Donaghy, T.Q.; Lamb, D.Q.; Sakamoto, T.; Norris, J.P.; Nakagawa, Y.; Villasenor, J.; Atteia, J.L.; Vanderspek, R.; Graziani, C.; Kawai, N.; et al. HETE-2 Localizations and Observations of Four Short Gamma-ray Bursts: GRBs 010326B, 040802, 051211 and 060121. *arXiv* **2006**, arXiv:astro-ph/0605570.
27. Horváth, I. A Third Class of Gamma-ray Bursts? *Astrophys. J.* **1998**, *508*, 757–759. [CrossRef]
28. Horváth, I. Classification of BeppoSAX's gamma-ray bursts. *Astrophys. Space Sci.* **2009**, *323*, 83–86. [CrossRef]
29. Řípa, J.; Wigger, C.; Huja, D.; Hudec, R. Gamma-ray Burst Classes Found in the Rhessi Data Sample. *Baltic Astron.* **2009**, *18*, 305–310.
30. Huja, D.; Mészáros, A.; Řípa, J. A comparison of the gamma-ray bursts detected by BATSE and Swift. *Astron. Astrophys.* **2009**, *504*, 67–71. [CrossRef]
31. Koen, C.; Bere, A. On multiple classes of gamma-ray bursts, as deduced from autocorrelation functions or bivariate duration/hardness ratio distributions. *Mon. Not. R. Astron. Soc. Lett.* **2012**, *420*, 405–415. [CrossRef]
32. Zitouni, H.; Guessoum, N.; Azzam, W.J.; Mochkovitch, R. Statistical study of observed and intrinsic durations among BATSE and Swift/BAT GRBs. *Astrophys. Space Sci.* **2015**, *357*, 7. [CrossRef]

33. Horváth, I.; Tóth, B.G. The duration distribution of Swift Gamma-ray Bursts. *Astrophys. Space Sci.* **2016**, *361*, 155. [CrossRef]
34. Tarnopolski, M. Analysis of the observed and intrinsic durations of gamma-ray bursts with known redshift. *Astrophys. Space Sci.* **2016**, *361*, 125. [CrossRef]
35. Kulkarni, S.; Desai, S. Classification of gamma-ray burst durations using robust model-comparison techniques. *Astrophys. Space Sci.* **2017**, *362*, 70. [CrossRef]
36. Tarnopolski, M. Distinguishing short and long Fermi gamma-ray bursts. *Mon. Not. R. Astron. Soc. Lett.* **2015**, *454*, 1132–1139. [CrossRef]
37. Tarnopolski, M. Analysis of gamma-ray burst duration distribution using mixtures of skewed distributions. *Mon. Not. R. Astron. Soc.* **2016**, *458*, 2024–2031. [CrossRef]
38. Band, D.L. Gamma-ray Burst Spectral Evolution through Cross-Correlations of Discriminator Light Curves. *Astrophys. J.* **1997**, *486*, 928–937. [CrossRef]
39. Von Kienlin, A.; Meegan, C.A.; Paciesas, W.S.; Bhat, P.N.; Bissaldi, E.; Briggs, M.S.; Burns, E.; Cleveland, W.H.; Gibby, M.H.; Giles, M.M.; et al. The Fourth Fermi-GBM Gamma-ray Burst Catalog: A Decade of Data. *Astrophys. J.* **2020**, *893*, 46. [CrossRef]
40. Goldstein, A.; Cleveland, W.H.; Kocevski, D. Fermi GBM Data Tools: v1.1.1. 2020. Available online: https://fermi.gsfc.nasa.gov/ssc/data/analysis/gbm (accessed on 17 June 2022).
41. Mukherjee, S.; Feigelson, E.D.; Jogesh Babu, G.; Murtagh, F.; Fraley, C.; Raftery, A. Three Types of Gamma-ray Bursts. *Astrophys. J.* **1998**, *508*, 314–327. [CrossRef]
42. Chattopadhyay, T.; Misra, R.; Chattopadhyay, A.K.; Naskar, M. Statistical Evidence for Three Classes of Gamma-ray Bursts. *Astrophys. J.* **2007**, *667*, 1017–1023. [CrossRef]
43. Modak, S. Distinction of groups of gamma-ray bursts in the BATSE catalog through fuzzy clustering. *Astron. Comput.* **2021**, *34*, 100441. [CrossRef]
44. Chattopadhyay, S.; Maitra, R. Gaussian-mixture-model-based cluster analysis finds five kinds of gamma-ray bursts in the BATSE catalogue. *Mon. Not. R. Astron. Soc. Lett.* **2017**, *469*, 3374–3389. [CrossRef]
45. Chattopadhyay, S.; Maitra, R. Multivariate t-mixture-model-based cluster analysis of BATSE catalogue establishes importance of all observed parameters, confirms five distinct ellipsoidal sub-populations of gamma-ray bursts. *Mon. Not. R. Astron. Soc. Lett.* **2018**, *481*, 3196–3209. [CrossRef]
46. Tóth, B.G.; Rácz, I.I.; Horváth, I. Gaussian-mixture-model-based cluster analysis of gamma-ray bursts in the BATSE catalog. *Mon. Not. R. Astron. Soc. Lett.* **2019**, *486*, 4823–4828. [CrossRef]
47. Balastegui, A.; Ruiz-Lapuente, P.; Canal, R. Reclassification of gamma-ray bursts. *Mon. Not. R. Astron. Soc. Lett.* **2001**, *328*, 283–290. [CrossRef]
48. Hakkila, J.; Haglin, D.J.; Pendleton, G.N.; Mallozzi, R.S.; Meegan, C.A.; Roiger, R.J. Gamma-ray Burst Class Properties. *Astrophys. J.* **2000**, *538*, 165–180. [CrossRef]
49. Hakkila, J.; Giblin, T.W.; Roiger, R.J.; Haglin, D.J.; Paciesas, W.S.; Meegan, C.A. How Sample Completeness Affects Gamma-ray Burst Classification. *Astrophys. J.* **2003**, *582*, 320–329. [CrossRef]
50. Rajaniemi, H.; Mähönen, P. Classifying gamma-ray bursts using self-organizing maps. *Astrophys. J.* **2002**, *566*, 202. [CrossRef]
51. Tarnopolski, M. Analysis of the Duration-Hardness Ratio Plane of Gamma-ray Bursts Using Skewed Distributions. *Astrophys. J.* **2019**, *870*, 105. [CrossRef]
52. Tarnopolski, M. Multivariate Analysis of BATSE Gamma-ray Burst Properties Using Skewed Distributions. *Astrophys. J.* **2019**, *887*, 97. [CrossRef]
53. Veres, P.; Bagoly, Z.; Horváth, I.; Mészáros, A.; Balázs, L.G. A Distinct Peak-flux Distribution of the Third Class of Gamma-ray Bursts: A Possible Signature of X-ray Flashes? *Astrophys. J.* **2010**, *725*, 1955–1964. [CrossRef]
54. Bhave, A.; Kulkarni, S.; Desai, S.; Srijith, P.K. Two Dimensional Clustering of Gamma-ray Bursts using durations and hardness. *arXiv* **2017**, arXiv:1708.05668.
55. Tsutsui, R.; Shigeyama, T. On the subclasses in Swift long gamma-ray bursts: A clue to different central engines. *Publ. Astron. Soc. Jpn.* **2014**, *66*, 42. [CrossRef]
56. Horváth, I.; Tóth, B.G.; Hakkila, J.; Tóth, L.V.; Balázs, L.G.; Rácz, I.I.; Pintér, S.; Bagoly, Z. Classifying GRB 170817A/GW170817 in a Fermi duration-hardness plane. *Astrophys. Space Sci.* **2018**, *363*, 53. [CrossRef]
57. Acuner, Z.; Ryde, F. Clustering of gamma-ray burst types in the Fermi GBM catalogue: Indications of photosphere and synchrotron emissions during the prompt phase. *Mon. Not. R. Astron. Soc. Lett.* **2018**, *475*, 1708–1724. [CrossRef]
58. Horváth, I.; Hakkila, J.; Bagoly, Z.; Tóth, L.V.; Rácz, I.I.; Pintér, S.; Tóth, B.G. Multidimensional analysis of Fermi GBM gamma-ray bursts. *Astrophys. Space Sci.* **2019**, *364*, 105. [CrossRef]
59. Modak, S.; Chattopadhyay, A.K.; Chattopadhyay, T. Clustering of Gamma-ray bursts through kernel principal component analysis. *arXiv* **2017**, arXiv:1703.05532.
60. Horváth, I. A further study of the BATSE Gamma-ray Burst duration distribution. *Astron. Astrophys.* **2002**, *392*, 791–793. [CrossRef]
61. Zhang, Z.B.; Yang, E.B.; Choi, C.S.; Chang, H.Y. Classifying gamma-ray bursts with Gaussian Mixture Model. *Mon. Not. R. Astron. Soc. Lett.* **2016**, *462*, 3243–3254. [CrossRef]
62. Horváth, I.; Balázs, L.G.; Bagoly, Z.; Veres, P. Classification of Swift's gamma-ray bursts. *Astron. Astrophys.* **2008**, *489*, L1–L4. [CrossRef]

63. Zhang, Z.B.; Choi, C.S. An analysis of the durations of Swift gamma-ray bursts. *Astron. Astrophys.* **2008**, *484*, 293–297. [CrossRef]
64. Horváth, I.; Bagoly, Z.; Balázs, L.G.; de Ugarte Postigo, A.; Veres, P.; Mészáros, A. Detailed Classification of Swift's Gamma-ray Bursts. *Astrophys. J.* **2010**, *713*, 552–557. [CrossRef]
65. Yang, E.B.; Zhang, Z.B.; Jiang, X.X. Two dimensional classification of the Swift/BAT GRBs. *Astrophys. Space Sci.* **2016**, *361*, 257. [CrossRef]
66. Zitouni, H.; Guessoum, N.; AlQassimi, K.M.; Alaryani, O. Distributions of pseudo-redshifts and durations (observed and intrinsic) of Fermi GRBs. *Astrophys. Space Sci.* **2018**, *363*, 223. [CrossRef]
67. Řípa, J.; Mészáros, A.; Veres, P.; Park, I.H. On the Spectral Lags and Peak Counts of the Gamma-ray Bursts Detected by the RHESSI Satellite. *Astrophys. J.* **2012**, *756*, 44. [CrossRef]
68. Minaev, P.Y.; Pozanenko, A.S.; Loznikov, V.M. Short gamma-ray bursts in the SPI-ACS INTEGRAL experiment. *Astrophys. Bull.* **2010**, *65*, 326–333. [CrossRef]
69. Svinkin, D.S.; Aptekar, R.L.; Golenetskii, S.V.; Frederiks, D.D.; Ulanov, M.V.; Tsvetkova, A.E. Classification of gamma-ray bursts observed with Konus-Wind. *J. Phys. Conf. Ser.* **2019**, *1400*, 022010. [CrossRef]
70. Minaev, P.Y.; Pozanenko, A.S. The $E_{p,I}$-E_{iso} correlation: Type I gamma-ray bursts and the new classification method. *Mon. Not. R. Astron. Soc. Lett.* **2020**, *492*, 1919–1936. [CrossRef]
71. Lü, H.J.; Zhang, B.; Liang, E.W.; Zhang, B.B.; Sakamoto, T. The 'amplitude' parameter of gamma-ray bursts and its implications for GRB classification. *Mon. Not. R. Astron. Soc. Lett.* **2014**, *442*, 1922–1929. [CrossRef]
72. Tarnopolski, M. How does the shape of gamma-ray bursts' pulses affect the duration distribution? *Mon. Not. R. Astron. Soc.* **2021**, *507*, 1450–1457. [CrossRef]
73. Tarnopolski, M. Can the Cosmological Dilation Explain the Skewness in the Gamma-ray Burst Duration Distribution? *Astrophys. J.* **2020**, *897*, 77. [CrossRef]
74. Baudry, J.P.; Raftery, A.E.; Celeux, G.; Lo, K.; Gottardo, R. Combining Mixture Components for Clustering. *J. Comput. Graph. Stat.* **2010**, *19*, 332–353. [CrossRef] [PubMed]
75. Kuhn, M.A.; Hillenbrand, L.A.; Carpenter, J.M.; Avelar Menendez, A.R. The Formation of a Stellar Association in the NGC 7000/IC 5070 Complex: Results from Kinematic Analysis of Stars and Gas. *Astrophys. J.* **2020**, *899*, 128. [CrossRef]
76. Lien, A.; Sakamoto, T.; Barthelmy, S.D.; Baumgartner, W.H.; Cannizzo, J.K.; Chen, K.; Collins, N.R.; Cummings, J.R.; Gehrels, N.; Krimm, H.A.; et al. The Third Swift Burst Alert Telescope Gamma-ray Burst Catalog. *Astrophys. J.* **2016**, *829*, 7. [CrossRef]
77. Fraley, C. *HDoutliers: Leland Wilkinson's Algorithm for Detecting Multidimensional Outliers*, R Package Version 1.0.2. 2020. Available online: https://CRAN.R-project.org/package=HDoutliers (accessed on 17 June 2022).
78. Scrucca, L.; Fop, M.; Murphy, T.B.; Raftery, A.E. mclust 5: Clustering, classification and density estimation using Gaussian finite mixture models. *R J.* **2016**, *8*, 289–317. [CrossRef]
79. Schwarz, G. Estimating the dimension of a model. *Ann. Stat.* **1978**, *6*, 461–464. [CrossRef]
80. Kass, R.E.; Raftery, A.E. Bayes Factors. *J. Am. Stat. Assoc.* **1995**, *90*, 773–795. [CrossRef]
81. Wang, N.; Raftery, A.E. Nearest-neighbor variance estimation (NNVE) robust covariance estimation via nearest-neighbor cleaning. *J. Am. Stat. Assoc.* **2002**, *97*, 994–1019. [CrossRef]
82. Walther, G. Detecting the presence of mixing with multiscale maximum likelihood. *J. Am. Stat. Assoc.* **2002**, *97*, 508–513. [CrossRef]
83. Li, J. Clustering based on a multilayer mixture model. *J. Comput. Graph. Stat.* **2005**, *14*, 547–568. [CrossRef]
84. Tantrum, J.; Murua, A.; Stuetzle, W. Assessment and pruning of hierarchical model based clustering. In Proceedings of the 9th ACM SIGKDD International Conference on Knowledge Discovery and Data Mining, Washington, DC, USA, 24–27 August 2003; pp. 197–205.
85. Sakamoto, T.; Barthelmy, S.D.; Baumgartner, W.H.; Cummings, J.R.; Fenimore, E.E.; Gehrels, N.; Krimm, H.A.; Markwardt, C.B.; Palmer, D.M.; Parsons, A.M.; et al. The Second Swift Burst Alert Telescope Gamma-ray Burst Catalog. *Astrophys. J. Suppl. Ser.* **2011**, *195*, 2. [CrossRef]
86. Bromberg, O.; Nakar, E.; Piran, T.; Sari, R. Short versus Long and Collapsars versus Non-collapsars: A Quantitative Classification of Gamma-ray Bursts. *Astrophys. J.* **2013**, *764*, 179. [CrossRef]
87. Bhat, P.N.; Meegan, C.A.; von Kienlin, A.; Paciesas, W.S.; Briggs, M.S.; Burgess, J.M.; Burns, E.; Chaplin, V.; Cleveland, W.H.; Collazzi, A.C.; et al. The Third Fermi GBM Gamma-ray Burst Catalog: The First Six Years. *Astrophys. J. Suppl. Ser.* **2016**, *223*, 28. [CrossRef]
88. Dainotti, M.G.; Lenart, A.Ł.; Sarracino, G.; Nagataki, S.; Capozziello, S.; Fraija, N. The X-Ray Fundamental Plane of the Platinum Sample, the Kilonovae, and the SNe Ib/c Associated with GRBs. *Astrophys. J.* **2020**, *904*, 97. [CrossRef]
89. Dainotti, M.G.; Livermore, S.; Kann, D.A.; Li, L.; Oates, S.; Yi, S.; Zhang, B.; Gendre, B.; Cenko, B.; Fraija, N. The Optical Luminosity-Time Correlation for More than 100 Gamma-ray Burst Afterglows. *Astrophys. J.* **2020**, *905*, L26. [CrossRef]
90. Dainotti, M.G.; Nagataki, S.; Maeda, K.; Postnikov, S.; Pian, E. A study of gamma ray bursts with afterglow plateau phases associated with supernovae. *Astron. Astrophys.* **2017**, *600*, A98. [CrossRef]
91. Gendre, B.; Joyce, Q.T.; Orange, N.B.; Stratta, G.; Atteia, J.L.; Boër, M. Can we quickly flag ultra-long gamma-ray bursts? *Mon. Not. R. Astron. Soc. Lett.* **2019**, *486*, 2471–2476. [CrossRef]
92. Gibson, S.L.; Wynn, G.A.; Gompertz, B.P.; O'Brien, P.T. Fallback accretion on to a newborn magnetar: Short GRBs with extended emission. *Mon. Not. R. Astron. Soc. Lett.* **2017**, *470*, 4925–4940. [CrossRef]

93. Kaneko, Y.; Bostancı, Z.F.; Göğüş, E.; Lin, L. Short gamma-ray bursts with extended emission observed with Swift/BAT and Fermi/GBM. *Mon. Not. R. Astron. Soc. Lett.* **2015**, *452*, 824–837. [CrossRef]
94. Gompertz, B.P.; O'Brien, P.T.; Wynn, G.A.; Rowlinson, A. Can magnetar spin-down power extended emission in some short GRBs? *Mon. Not. R. Astron. Soc. Lett.* **2013**, *431*, 1745–1751. [CrossRef]
95. Gompertz, B.P.; O'Brien, P.T.; Wynn, G.A. Magnetar powered GRBs: Explaining the extended emission and X-ray plateau of short GRB light curves. *Mon. Not. R. Astron. Soc. Lett.* **2014**, *438*, 240–250. [CrossRef]
96. Ashall, C.; Mazzali, P.A.; Pian, E.; Woosley, S.E.; Palazzi, E.; Prentice, S.J.; Kobayashi, S.; Holmbo, S.; Levan, A.; Perley, D.; et al. GRB 161219B/SN 2016jca: A powerful stellar collapse. *Mon. Not. R. Astron. Soc. Lett.* **2019**, *487*, 5824–5839. [CrossRef]
97. Melandri, A.; Malesani, D.B.; Izzo, L.; Japelj, J.; Vergani, S.D.; Schady, P.; Sagués Carracedo, A.; de Ugarte Postigo, A.; Anderson, J.P.; Barbarino, C.; et al. GRB 171010A/SN 2017htp: A GRB-SN at z = 0.33. *Mon. Not. R. Astron. Soc. Lett.* **2019**, *490*, 5366–5374. [CrossRef]
98. Izzo, L.; Rossi, A.; Malesani, D.; Heintz, K.; Selsing, J.; Schady, P.; Starling, R.; Sollerman, J.; Leloudas, G.; Cano, Z.; et al. GRB 180728A: Discovery of the associated supernova. *GRB Coord. Netw.* **2018**, *23142*, 1.
99. Selsing, J.; Izzo, L.; Rossi, A.; Malesani, D.; Heintz, K.; Schady, P.; Starling, R.; Sollerman, J.; Leloudas, G.; Cano, Z.; et al. GRB 180728A: Classification of the associated SN 2018fip. *GRB Coord. Netw.* **2018**, *23181*, 1.
100. Hu, Y.D.; Castro-Tirado, A.J.; Kumar, A.; Gupta, R.; Valeev, A.F.; Pandey, S.B.; Kann, D.A.; Castellón, A.; Agudo, I.; Aryan, A.; et al. 10.4 m GTC observations of the nearby VHE-detected GRB 190829A/SN 2019oyw. *Astron. Astrophys.* **2021**, *646*, A50. [CrossRef]
101. Jespersen, C.K.; Severin, J.B.; Steinhardt, C.L.; Vinther, J.; Fynbo, J.P.U.; Selsing, J.; Watson, D. An Unambiguous Separation of Gamma-ray Bursts into Two Classes from Prompt Emission Alone. *Astrophys. J.* **2020**, *896*, L20. [CrossRef]
102. Salmon, L.; Martin-Carrillo, A.; Hanlon, L. Two Classes of Gamma-ray Bursts Distinguished within the First Second of Their Prompt Emission. *Galaxies* 2022, *submitted*. [CrossRef]
103. Harris, C.R.; Millman, K.J.; van der Walt, S.J.; Gommers, R.; Virtanen, P.; Cournapeau, D.; Wieser, E.; Taylor, J.; Berg, S.; Smith, N.J.; et al. Array programming with NumPy. *Nature* **2020**, *585*, 357–362. [CrossRef]
104. Hunter, J.D. Matplotlib: A 2D graphics environment. *Comput. Sci. Eng.* **2007**, *9*, 90–95. [CrossRef]
105. Pandas Development Team. *Pandas-Dev/pandas*, Pandas-v1.4.2. 2020. Available online: https://doi.org/10.5281/zenodo.3509134 (accessed on 17 June 2022).
106. Wes McKinney. Data Structures for Statistical Computing in Python. In Proceedings of the 9th Python in Science Conference, Austin, TX, USA, 28 June–3 July 2010; van der Walt, S., Millman, J., Eds.; SciPy: Austin, TX, USA, 2010; pp. 56–61. [CrossRef]